Treatment Efficacy for Validating MicroCT-Based Theoretical Simulation Approach in Magnetic Nanoparticle Hyperthermia for Cancer Treatment

Alexander LeBrun
Department of Mechanical Engineering,
University of Maryland Baltimore County,
Baltimore, MD 21250

Tejashree Joglekar
Department of Biology,
University of Maryland Baltimore County,
Baltimore, MD 21250

Charles Bieberich
Department of Biology,
University of Maryland Baltimore County,
Baltimore, MD 21250

Ronghui Ma
Department of Mechanical Engineering,
University of Maryland Baltimore County,
Baltimore, MD 21250

Liang Zhu[1]
Department of Mechanical Engineering,
University of Maryland Baltimore County,
1000 Hilltop Circle,
Baltimore, MD 21250
e-mail: zliang@umbc.edu

The objective is to validate a designed heating protocol in a previous study based on treatment efficacy of magnetic nanoparticle hyperthermia in prostate tumors. In vivo experiments have been performed to induce temperature elevations in implanted PC3 tumors injected with magnetic nanoparticles, following the same heating protocol designed in our previous microCT-based theoretical simulation. A tumor shrinkage study and histological analyses of tumor cell death are conducted after the heating. Tumor shrinkage is observed over a long period of 8 weeks. Histological analyses of the tumors after heating are used to evaluate whether irreversible thermal damage occurs in the entire tumor region. It has been shown that the designed 25 min heating (Arrhenius integral $\Omega \geq 4$ in the entire tumor) on tumor tissue is effective to cause irreversible thermal damage to PC3 tumors, while reducing the heating time to 12 min ($\Omega \geq 1$ in the entire tumor) results in an initial shrinkage, however, later tumor recurrence. The treated tumors with 25 min of heating disappear after only a few days. On the other hand, the tumors in the control group without heating show approximately an increase of more than 700% in volume over the 8-week observation period. In the undertreated group with 12 min of heating, its growth rate is smaller than that in the control group. In addition, results of the histological analysis suggest vast regions of apoptotic and necrotic cells, consistent with the regions of significant temperature elevations. In conclusion, this study demonstrates the importance of imaging-based design for individualized treatment planning. The success of the designed heating protocol for completely damaging PC3 tumors validates the theoretical models used in planning heating treatment in magnetic nanoparticle hyperthermia. [DOI: 10.1115/1.4035246]

Keywords: magnetic nanoparticle hyperthermia, treatment efficacy, tumor shrinkage, histological analysis, bioheat transfer

1 Introduction

Hyperthermia treatment using physical modalities has attracted a lot of attention in the past decades in cancer treatment, as an alternative to patients who have compromised health and cannot go through traditional cancer treatment methods. The amount of thermal damage to tumor cells is usually affected by the extent of temperature elevations in the tissue and its exposure time [1,2]. Among all the thermal ablation techniques, magnetic nanoparticles have gained prominence in the last two decades for use in hyperthermia, in additional to their clinical applications such as drug delivery and medical imaging. In magnetic nanoparticle hyperthermia, an external alternating magnetic field is applied to the nanoparticles to generate localized heating in targeted tissue region. Designing an optimal heating protocol to cause irreversible thermal damage to tumors while preserving the surrounding healthy tissue relies on a wide range of heating parameters such as magnetic field strength, frequency, local concentration of nanoparticles, and heating duration. The designed heating protocol also depends on the specific cell line, growth stage, and their surrounding tissue environment. Evaluating a designed heating protocol using magnetic nanoparticles in animal models is the first step to test its efficacy in a biological environment, leading to validation of the theoretical modeling approach for future optimal designs in clinical settings.

Various models have been proposed to assess thermal damage, taking into consideration the complicated biological and chemical reactions during heating [3,4]. Among them, the Arrhenius integral Ω is developed based on the first-order chemical reaction equation to assess cell death [3]. A recent study [4] has suggested that implementation of a temperature-dependent time delay to the traditional Arrhenius model significantly improves agreement between experimental measurements of cell death and model prediction. The values of the coefficients shown in those models are typically determined from experimental studies when a specific tumor cells are placed in a fixed temperature environment for a specific duration. The major challenge is that the magnitudes of the coefficients can be affected by many factors, since tolerance to heat varies from one type of cells to another, and also depends on growth stages of the cells [5]. Another challenge is that these coefficients may also be affected by the level of temperature elevations and its distribution achieved during treatment. One study shows that physiological responses of tumors to mild hyperthermia (40–43 °C), including increases in tumor blood flow and heat

[1]Corresponding author.

Presented at the 2016 ASME 5th Micro/Nanoscale Heat & Mass Transfer International Conference. Paper No. MNHMT2016-6559.

Contributed by the Heat Transfer Division of ASME for publication in the JOURNAL OF HEAT TRANSFER. Manuscript received April 6, 2016; final manuscript received October 24, 2016; published online February 7, 2017. Assoc. Editor: Chun Yang.

shock protein expression, can greatly affect the treatment outcome [6]. It has been suggested that administration of a large thermal dosage can elevate local temperatures greater than 50 °C for a short duration of time and can reduce the impact of these physiological responses for more controllable treatment outcomes [7].

Another approach to evaluate thermal damage is via tumor shrinkage after hyperthermia treatment [8]. Tumor shrinkage after a treatment and maintenance of the shrinkage for a sufficiently long time are indication of irreversible thermal damage to cells. On the other hand, damage at the cellular level is only recognizable based on pathological evaluations of treated tissue. These histological markers reveal whether the temperature elevation and duration of heating result in recoverable damage or lethal thermal effects, something that cannot be determined by inspection of a shrinking tumor. Recoverable damages, such as intracellular edema, thermal inactivation of specific enzymes, as well as cellular membrane rupture, represent situations when cells may tolerate and survive the modest temperature elevations for specific periods of heating after the treatment [9]. Other lethal thermal markers include necrosis (trauma induced cell death) and apoptosis (programmed cell death). These occur when the repair mechanisms or their mediators (deoxyribonucleic acid and ribonucleic acid enzymes) are affected due to the imposed thermal stresses [10]. After a heating treatment, the release of heat shock proteins (HSPs) can also be regarded as an indication of cell necrosis or cellular stress [2]. Therefore, observation of various markers in histological analyses can be used to evaluate severity and uniformity of thermal damage to entire tumors.

One of the most commonly used methods to quantify morphological changes in the cellular structure is to perform hematoxylin and eosin (H&E) staining [11]. H&E staining is also commonly used during biopsies to determine whether cancer is present since many forms of cancer cells are poorly differentiated, i.e., they do not resemble normal cells, from the surrounding healthy cell. Using this process, basophilic/negatively charged structures such as deoxyribonucleic acid, ribosomes, and the cell nucleus are stained a bluish color while eosinophilic/positively charged structures such as cytoplasm and extracellular proteins like collagen are stained a pinkish color.

In a previous study of our group [12], heating protocols are designed to determine the heating time to induce complete thermal damage to PC3 tumors implanted on mice, with minimal collateral damage to the surrounding healthy mouse tissue below an acceptable level. The heating protocols are determined from microCT scan-generated tumor geometry and heat generation distribution. The Arrhenius integral Ω is calculated based on tumor temperature field simulation to determine how long it takes to achieve a design objective of $\Omega \geq 1$ or 4 in the entire tumor implanted on a mouse. Based on using the same magnetic field strength and the same ferrofluid infusion rate and amount, a heating time of 12 min or 25 min is determined to achieve $\Omega \geq 1$ or 4 in the entire PC3 tumors. Although many previous studies use both criteria as the threshold of irreversible thermal damage, $\Omega \geq 1$ only implies 63% of the cell death based on the Arrhenius integral, while $\Omega \geq 4$ suggests 98.2% of the cell death after the heating duration. It is not clear whether 63% of the cell death in tumors is sufficient to induce irreversible thermal damage to the entire tumor. In other words, it remains a question whether the remaining 37% of tumor cells would recover from the heating treatment. In addition, none of the previous studies evaluated both thresholds simultaneously in PC3 tumors to investigate the treatment efficacy using magnetic nanoparticle hyperthermia.

The goals of this study are to measure tumor shrinkage and to perform histological analyses after magnetic nanoparticle hyperthermia, and to evaluate whether the designed heating protocol indeed induces adequate thermal damage to tumors. Tumor shrinkage/growth will be observed over a long period of 8 weeks. Histological analyses of the tumors after treatment will be used to evaluate whether irreversible thermal damage occurs in the entire tumor region.

2 Methods and Materials

2.1 Heating Experiment. Twenty-two BALB/c Nu/Nu female mice (25 ± 2.6 g) between 4 and 6 weeks in age were used to test the efficacy of the designed heating protocol. Once the tumors have reached a minimum diameter of 1 cm, the mice were weighed and anesthetized using sodium pentobarbital (40 mg/kg, i.p.). The mouse was then placed on a water-jacketed heating pad to maintain the normal body core temperature. Some tumors were injected with 0.1 cc of the commercially available ferrofluid used previously at a rate of 3 μL/min, following the procedures described in a previous study [13], while other tumors were used as the control. After the injection, the needle was removed and the mouse was placed inside a two-turn water-cooled coil on the water-jacketed heating pad. The alternating magnetic field induced by the coil has a magnetic strength of approximately 5 kA/m and a frequency of 190 kHz [13]. The experimental setup of this study can be seen in Fig. 1. The appropriate heating duration was determined using the computational models in a previous study [12], and the heating time was either 25 min or 12 min when the Arrhenius integral $\Omega \geq 4$ or 1, respectively, in the entire tumor.

2.2 Tumor Shrinkage Study. Three groups (five tumors in each group) were tested for this part of the study: 25 min of heating (the Arrhenius integral $\Omega \geq 4$), 12 min of heating ($\Omega \geq 1$), and the control group with no nanoparticles but subjected to the alternating magnetic field for 25 min. After the heating experiment, the mouse was allowed to fully recover before it was returned to the animal facility at UMBC, following the protocol approved by the IACUC. The tumor growth/shrinkage was measured daily over the next 8 weeks using a Vernier caliper. Previous studies [12,14–17] suggested a modified ellipsoidal formula to approximate the volume of the tumor

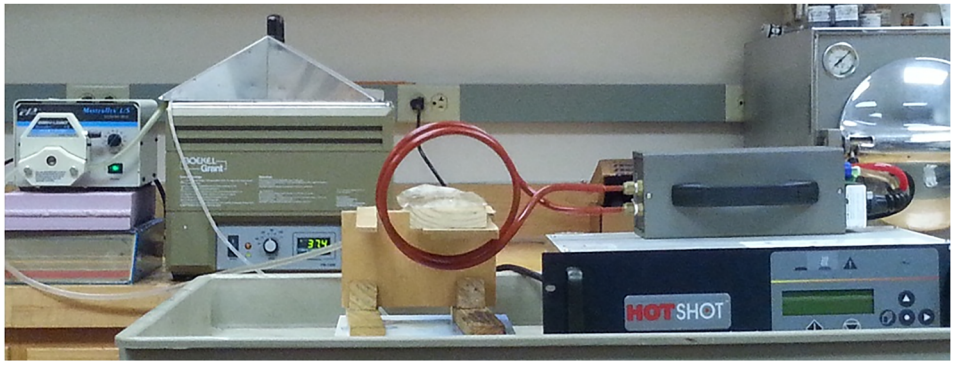

Fig. 1 Experimental setup of the study, including an RF generator, a two-turn coil to induce an alternating magnetic field, a stage for holding the mouse, a water circulating heating pad, a pump, and a water reservoir supplying 37 °C warm water

$$\text{tumor volume} = \frac{1}{2}(L \times W^2) \quad (1)$$

where L is the greatest longitudinal diameter (mm) and W is the greatest transverse diameter (mm). This method has been shown to provide an accurate volume estimation of the tumor volume from comparisons with that measured by three-dimensional microCT scans and positron emission tomography (PET) imaging technology [18]. After the tumor shrinkage study was completed, all mice were euthanized via a sodium pentobarbital overdose (160 mg/kg, i.p.).

2.3 Histological Analysis. Seven BALB/c Nu/Nu female mice were used for histological analysis (28.1 ± 1.6 g) with an average tumor size of 0.96 ± 0.15 mm^3. Histological analyses were performed on three groups: two tumors with neither nanoparticles nor heating (the control group), two tumors injected with magnetic nanoparticles with no heating (the sham group), and three tumors with nanoparticle injection and subject to 25 min of heating (the heating group). After the experiment, the mouse was euthanized via a sodium pentobarbital overdose (160 mg/kg, i.p.), and the tumor was resected. To determine the extent of thermal damage in the tumor, H&E staining was performed on 5 μm sections cut from the tumors preserved in the 10% neutral buffered formalin (NBF) solution. H&E staining is routinely used by pathologists because it offers detailed view of cellular structures of the otherwise transparent tissue. This method can clearly stain cell structures such as the cytoplasm, nucleus, organelles, and extracellular components either red or blue depending on the charge. For each specimen, one slide was stained and six slides were left unstained for pathological analysis.

3 Results

3.1 Tumor Shrinkage Study. As shown in Table 1, the initial sizes of the treated groups are similar, allowing for more appropriate comparisons between the two heating groups. The tumor size in the control group was smaller to allow for more time to grow the tumors. For a mouse with bilateral tumors, if one of the tumors was too large, the mouse had to be euthanized.

The shrinkages/growths of the tumors in all three groups are plotted in Figs. 2–4. Student's t-test was used to determine if there was significant growth (or regression) of the tumor over the 8-week observation period, using the tumor volume on the first day as a reference. As shown in Fig. 2, the tumors in the control group without heating almost double their sizes within 10 days, and at the end of the observation period of 8 weeks, the volume increases from the initial 300 mm^3 to 2600 mm^3. In the Arrhenius integral assessing thermal damage, $\Omega = 1$ implies that 63% of the tumor cells will be damaged; however, it is possible that the remaining 37% of the tumor cells may still be alive. When $\Omega = 1$ is selected as the damage threshold, the heating time is found as short as 12 min; therefore, this group can be considered as the barely minimal heating group or undertreated group. Figure 3 provides the

Table 1 Initial measured tumor sizes of the three groups

Tumor #	1	2	3	4	5
			Control group		
L (mm)	8.3	10.8	10.4	9.35	9.55
W (mm)	7	8.05	9.2	6.8	8.25
Volume (mm^3)	203.35	349.93	440.13	216.17	324.99
Mean ± SD (mm^3)			306.91 ± 98.59		
			Undertreated group (12 min)		
L (mm)	11.5	12.7	11.7	12.6	12.8
W (mm)	10.95	11.4	9.4	11.35	9.75
Volume (mm^3)	689.44	825.25	516.91	811.58	608.40
Mean ± SD (mm^3)			690.32 ± 131.99		
			Completely treated group (25 min)		
L (mm)	9.85	12.9	12.5	11.5	11.4
W (mm)	10.75	10.75	10.6	10.75	10.2
Volume (mm^3)	569.14	745.38	702.25	664.48	593.03
Mean ± SD (mm^3)			654.86 ± 73.66		

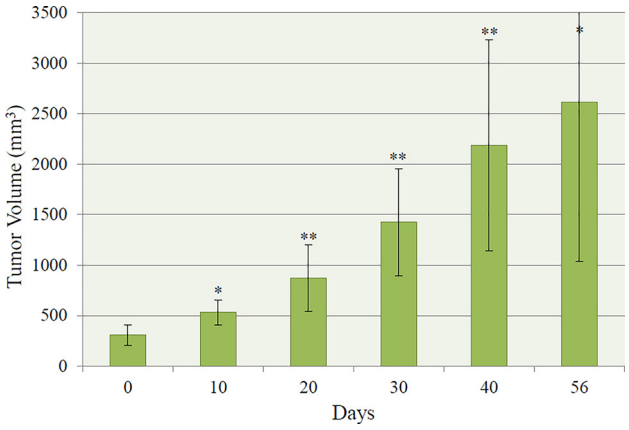

Fig. 2 Average tumor volumes and their standard deviations in the control group of tumors without ferrofluid injection over the 8-week observation period; * represents a *p*-value less than 0.05 and ** represents a *p*-value less than 0.01

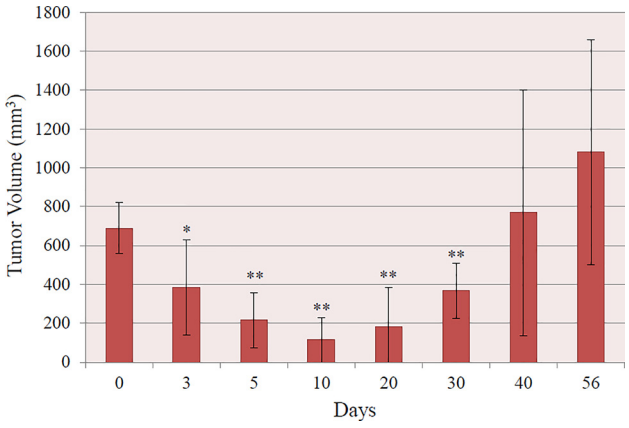

Fig. 3 Tumor shrinkage/growth over 8 weeks after 12 min of heating in the undertreated group; * represents a *p*-value less than 0.05 and ** represents a *p*-value less than 0.01

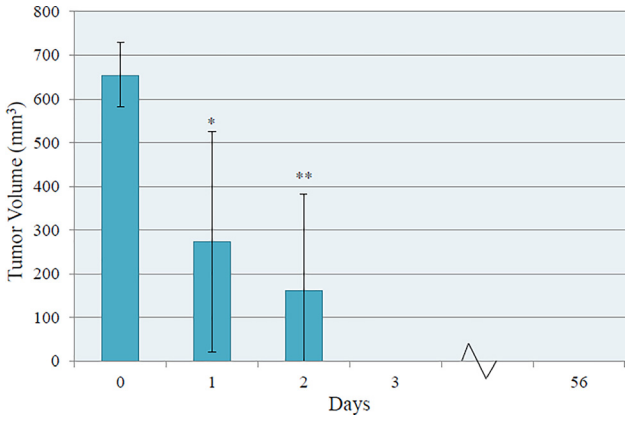

Fig. 4 Tumor shrinkage after 25 min of heating in the completely treated group; * represents a *p*-value less than 0.05 and ** represents a *p*-value less than 0.01

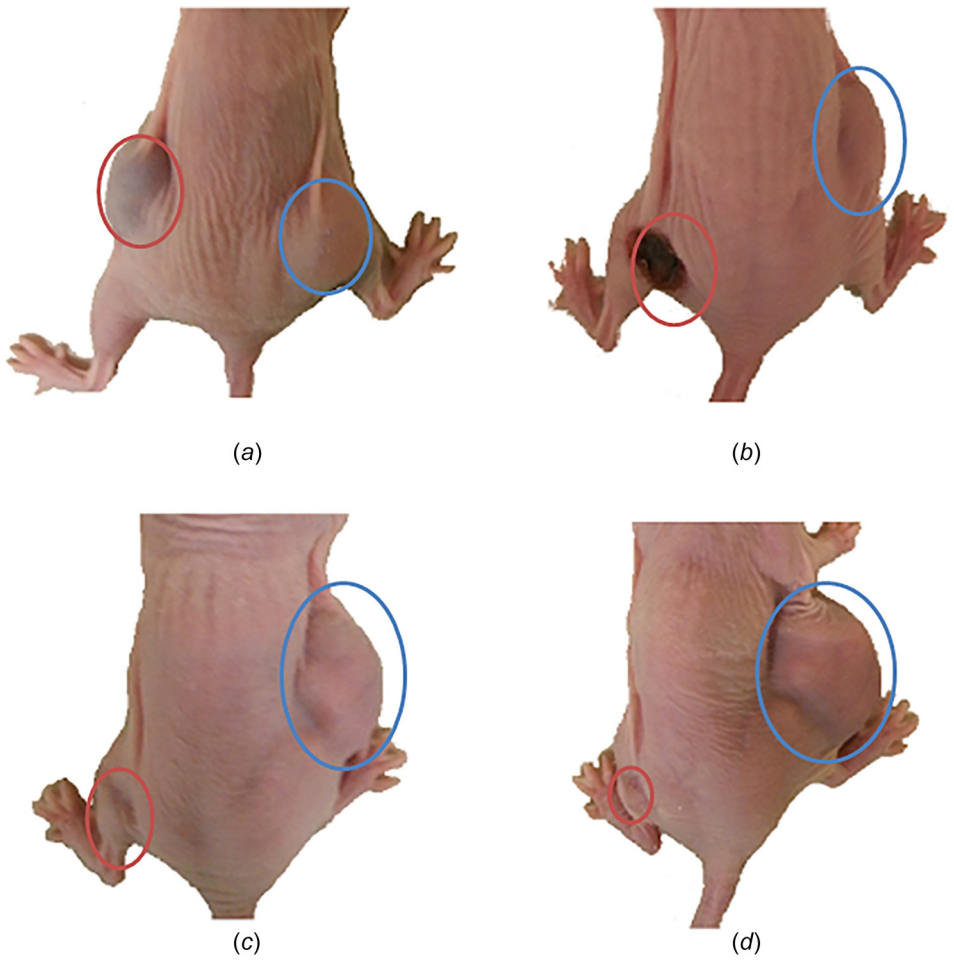

Fig. 5 Tumor growth and shrinkage at (*a*) pretreatment, (*b*) 2 weeks, (*c*) 4 weeks, and (*d*) 8 weeks posttreatment. The right circle in each panel represents the control tumor while the left circle represents the treated tumor with 25 min of heating.

tumor volume variations over the 8-week observation period. The average tumor volume shrinks 85% from the initial 655 mm^3 to 100 mm^3 within ten days, suggesting some positive outcomes in damaging tumor cells. Unfortunately, ten days after heating, the previously disappearing tumors start to grow back. Their average volume is almost the same as the initial size 40 days after the heating, and it reaches 1100 mm^3 56 days later, an almost 68% increase from the initial value.

In the $\Omega = 4$ heating group, the heating time is designed as 25 min, in order to achieve 98.2% death in tumor cells. The average tumor volume variations in the $\Omega = 4$ heating group after the heating treatment are plotted in Fig. 4. The tumors in the heating group of 25 min disappeared completely after the third day, and the treatment site maintained the disappearance for the 8-week observation period. The actual photos of the same mouse bearing two PC3 tumors are given in Fig. 5. After the tumor was treated, a burn at the treatment site was visible two weeks posttreatment. Two weeks later, the burn reduced to a small scar on the right flank. Eight weeks posttreatment, the mouse showed no observable tumor growth and only a small scar remained at the treatment site.

We further evaluate whether heating inhibits tumor growth, illustrated in Fig. 6. The tumor growth rate in the control group is slow at the very beginning, then accelerates in the middle (~55 mm^3/day), and finally reaches 140 mm^3/day by the end of the 8 weeks of observation, with an average growth rate of approximately 67 mm^3/day. In the undertreated group, the initial shrinkage rate (negative values in the figure) within the first ten days is approximately 80 mm^3/day by average, then the tumors grow back and the growth rates are noticed as approximately 35 mm^3/day in weeks 3–8 when the tumors grow back. The results suggest that heating inhibits tumor growth, although the thermal dosage in the undertreated group is not sufficient to obliterate the entire tumors. It is evident that with the high thermal dosage in the $\Omega = 4$ group, the initial shrinkage rate varies from 370 mm^3/

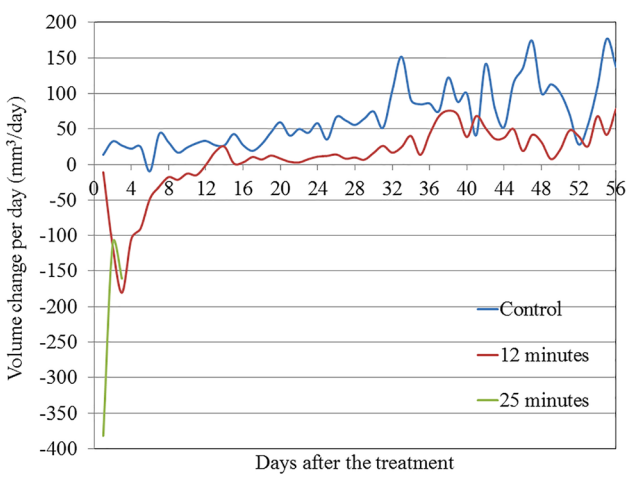

Fig. 6 Tumor growth rates (mm^3/day) in the three groups over the observation duration of 56 days

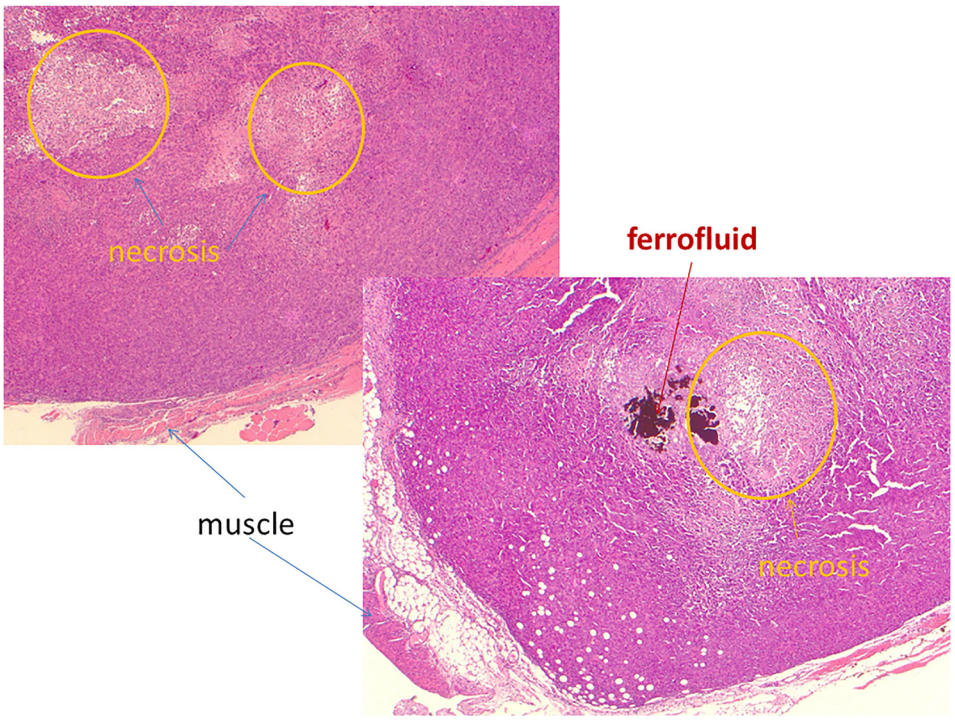

Fig. 7 H&E staining images of tumors at 25× magnification for the control group without heating (top panel) and the sham group (bottom panel). The scale bars are 1 mm. The circle shows the necrotic regions.

day in day 1 to 160 mm^3/day in day 3, without any further tumor regrowth after day 3. The average shrinkage rate in the $\Omega = 4$ group within the first 3 days is much higher than that in the under-treated group, therefore, accelerating the tumor shrinkage after heating.

3.2 Histological Analysis. The top panel in Fig. 7 provides the typical H&E staining of PC3 tumors with neither nanoparticle injection nor heating at the 25× magnification. Pictures were taken with a camera (AxioCam MRc5, Zeiss, Charlotte, NC) mounted on a microscope (BX51, Olympus, Tokyo, Japan) and processed using the software (AxioVision, Zeiss, Charlotte, NC) that came with the camera. The lower right-hand side shows the tumor periphery noted by the region of muscle. Under 25× magnification, it is evident that there are necrotic regions in the untreated tumor. Under normal conditions, the presence of necrotic region in PC3 tumors is not uncommon, and it is most likely due to poor blood supply to those regions and/or the aggressive growing nature of the particular tumor. The typical H&E staining of PC3 tumor tissue in the sham group only injected with ferrofluid, however, without heating, is shown in the bottom panel in Fig. 7. The PC3 tissue in the sham group still resembles normal PC3 cells. The black area in the stain is a small deposition of the ferrofluid. Note that during slicing of PC3 tumors, not all of the ferrofluid still holds in its original tumor region. It is evident that tumor necrosis still occurs in the tumors of the sham group. The presence of nanoparticles from the direct intratumoral injection does not seem to result in any additional cell necrosis to the tumor region. The tumor periphery still resembles normal PC3 cells with healthy fat and muscle layers.

Figure 8 shows the stained images of a tumor slice under 25× and 100× magnification after the tumor was heated for 25 min. Once heated, the tumor was immediately resected and suspended in 10% NBF to observe the early stages of cell death. The thick lines branching off the ferrofluid deposit toward the tumor periphery are artifacts, which have occurred because the structural integrity of the cells resulted in folds during the staining process. It can be clearly seen that there are several areas of tumor cells containing no discernable nuclei and areas of cells detaching from their surrounding cells. The stained nuclei and cytoplasm in Fig. 8 differ greatly from those in Fig. 7. The nuclei are significantly darker suggesting that the cells are pyknotic, a condensing of the nuclei that is pre-apoptotic or necrotic [9]. Cells in the immediate vicinity of the ferrofluid deposition region (dark region in the

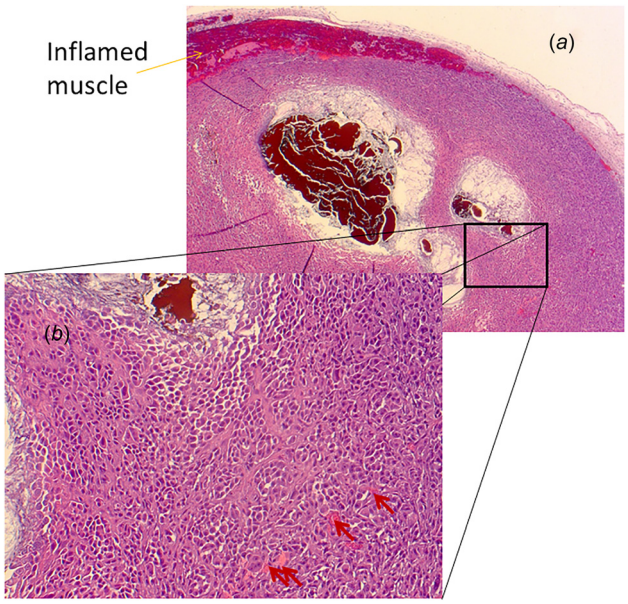

Fig. 8 Histologic images of immediately resected PC3 tumors after 25 min of heating (*a*) 25× and (*b*) 100× magnification. The scale bar in (*a*) is 1 mm and the scale bar in (*b*) is 200 μm. Arrows show red blood vessels.

center of the image) are indiscernible as the cell structures have been completely destroyed and they appear "liquefied," much different than the region surrounding the ferrofluid in Fig. 7. The muscle surrounding the periphery of the tumor also shows severe thermal damage due to heating, suggesting that heat penetration to the periphery regions is prevalent.

4 Discussion

It has been well demonstrated over the last decade that magnetic nanoparticle-induced hyperthermia has the potential of confining heat to targeted tumors. If sufficient nanoparticles are delivered to tumors, the tumors can be completely ablated with minimal collateral damage to the surrounding healthy tissue. Direct intratumoral injection of ferrofluid to tumors has the advantage over systemic (intravenous) delivery, since it can be effective to deposit nanoparticles to targeted tumors even if the tumors are poorly and/or nonuniformly perfused. Theoretical studies have shown the feasibility of elevating tumor temperatures to 50–80 °C, sufficient to induce irreversible damage to the cancerous tissue [12,19,20].

The major finding of this study is that the observed tumor shrinkage supports the hypothesis that the heating protocol achieves the objective of complete thermal damage to the tumors after being implemented, following the design. The group of tumors without treatment showed continuous volume growth over the observed time period, with its volume increasing up to ten times of their initial values in some cases. In the undertreated group, the tumors showed significant initial shrinkage (approximately 85% of its original volume) and later regrowth to more than its initial volume over an observation period of 8 weeks. However, the tumor growth rate was slowed down after heating. Only in the group of the treated tumors following the designed 25 min of heating, all tumors completely disappeared over the observed 8 weeks, and some tumors disappeared after a day or two. One significant improvement of this study is the long observation period of 8 weeks from previous tumor shrinkage studies of only 3 weeks or less [8,17]. This longer observation period is considered as a threshold, after which the tumor is unlikely to grow back.

Histological analyses of tumor cell death are another important part of this study to confirm the efficacy of the designed heating protocol. Histology of the control tumor shows that PC3 cells are aggressive in nature. It also shows that due to their aggressive nature, some tumor regions become necrotic possibly as the result of poor vascular structure at their later growth stages. The finding shows the importance of testing tumors at consistent growth stages to have more comparable results. Previous studies have studied toxicity of nanoparticles to tissue; however, those studies are focused on toxicity in liver or spleen due to nanoparticle uptake by those organs, usually in the systemic delivery of ferrofluid [21–24]. In direct intratumoral injections of ferrofluid, uptake in the liver or spleen due to nanoparticles getting into blood circulation is minimal. As for toxicity of nanoparticle to local tissue (including tumors), previous studies have suggested no toxicity when the local iron concentration in tissue ranges from 31 and 58.45 mg/g of tissue [25]. In our study, due to the very small volume concentration (5.8%) and the small amount of ferrofluid injected (0.1 cc), it is estimated that 0.1 cc only contains 25.2 mg of iron [13]. The histological analysis of this study seems confirming that toxicity of nanoparticles to PC3 tumors is negligible. In the sham group with ferrofluid injection only, although necrotic cells are noted in the immediate vicinity of the ferrofluid, the necrotic cell region is almost the same as that in the control group with neither ferrofluid injection nor heating. Therefore, it is unlikely that ferrofluid injection alone causes additional cell necrosis. The treated group shows serious necrosis and apoptosis in the tumor cells after immediate resection. With the thermal damage shown, it is expected that the tumor cells would not be able to recover. In the treated group, damages to muscle and fat near the tumor are noticed. This result is expected from the simulations since complete thermal damage also is predicted at tumor periphery.

One limitation of the study is that the tumor is resected right after the heating experiment for histological analyses. Typically, after the initial damage, indirect or delayed cellular damage may also occur due to cascading biochemical reactions triggered by the initial thermal damage. The damage may become evident several hours after the initial heating, and may last for several days. It includes microvascular damage leading to vascular stasis and thrombosis, cellular apoptosis due to nonuniform temperature elevations and altering of tumor microenvironment, secretion of tumor necrosis factors by Kupffer cells in the liver, and systemic production of cytokines [26–28]. In addition, after the initial damage, the tissue may start repairing mechanisms [29]. For example, high levels of heat shock proteins have been observed to be overexpressed in tumor cells in responding to heating [29]. It is known that heat shock proteins are used to salvage denatured proteins and promote cell survival. Therefore, if tumors were resected several hours after heating, the histological results might have been different from what we obtained, due to repairing mechanisms decreasing inflammation in the cells and/or secondary damage. More histological analyses at various time points after the initial heating are needed to quantitatively evaluate secondary damage and repairing responses.

Another limitation of the study is the use of a tumor model implanted beneath skin surfaces. It is unclear how accurately those tumor models capture human malignancy in deep-seated tumors, and whether the distribution of nanoparticles and thermal tolerance by tumors are affected by the tumor location. Future studies are warranted to test tumor models in situ for more clinically relevant results. In addition, the focus of this study is on the PC3 tumor, one of several human prostatic tumors affecting elder populations. Although the study has showed the effectiveness of using a heating protocol to induce permanent thermal damage to PC3 tumors, it may not indicate the effectiveness of the heating protocol to other forms of prostatic tumors such as DU145, LNCaP, C4-2, and C4-2B. Future experimental studies will be needed to determine tumor-type specific thermal dosages. The treatment protocol is designed based on the simulation results in a previous study. The implementation of the treatment protocol is based on the hypothesis that the nanoparticle distribution in PC3 tumors would be similar if one follows the same injection strategy [13]. To achieve a truly individualized treatment protocol design, one may use a microCT imaging system that allows in vivo imaging of the mouse with embedded tumors. This approach can be used to determine individualized heating duration based on size and nanoparticle distribution in the tumor, without sacrificing the mouse and tumor resection.

In summary, in vivo experiments have been performed to induce temperature elevations in implanted PC3 tumors in mice using magnetic nanoparticles following the same heating protocol designed in our theoretical study. A tumor shrinkage study and histological analyses of tumor cell death are conducted to confirm treatment efficacy of the designed heating protocol. It has been shown that 25 min heating on tumor tissue is effective to cause irreversible thermal damage to PC3 tumors while lowering the heating time results in an initial shrinkage, however, later tumor recurrence. The treated tumors with 25 min of heating disappear after only a few days. On the other hand, the tumors in the control group without heating show approximately an increase of more than 700% in volume over the 8-week observation period. In the undertreated group, an initial shrinkage is observed; however, the tumors grow back later, although its growth rate is smaller than that in the control group. In addition, results of the histological analysis suggest vast regions of apoptotic and necrotic cells, consistent with the regions of significant temperature elevations. In conclusion, this study demonstrates the importance of imaging-based design for individualized treatment planning. The success of the designed heating protocol for completely damaging PC3

tumors validates the theoretical models used in planning heating treatment in magnetic nanoparticle hyperthermia.

Acknowledgment

This study is support in part by an NSF research grant CBET-1335958 and the GAANN Scholarship Program at UMBC. The research is performed in partial fulfilment of the requirements for the Ph.D. degree from UMBC by Alexander LeBrun.

References

[1] Dewhirst, M. W., Viglianti, B. L., Lora-Michiels, M., Hanson, M., and Hoopes, P. J., 2003, "Basic Principles of Thermal Dosimetry and Thermal Thresholds for Tissue Damage From Hyperthermia," Int. J. Hyperthermia, **19**(3), pp. 267–294.
[2] Bia, J. F., Liu, P., and Xu, L. X., 2014, "Recent Advances in Thermal Treatment Techniques and Thermally Induced Immune Responses Against Cancer," IEEE Trans. Biomed. Eng., **61**(5), pp. 1497–1505.
[3] Moritz, A. R., and Henriques, F. C., 1947, "Studies of Thermal Injury II: the Relative Importance of Time and Surface Temperature in the Causation of Cutaneous Burns," Am. J. Pathol., **23**(5), pp. 695–720.
[4] Pearce, J. A., 2015, "Improving Accuracy in Arrhenius Models to Cell Death: Adding a Temperature-Dependent Time Delay," ASME J. Biomech. Eng., **137**(12), p. 121006.
[5] Ryu, S., Brown, S. L., Kim, S. H., Khil, M. S., and Kim, J. H., 1996, "Preferential Radiosensitization of Human Prostatic Carcinoma Cells by Mild Hyperthermia," Int. J. Radiat. Oncol. Biol. Phys., **34**(1), pp. 133–138.
[6] Rylander, M. N., Stafford, R. J., Hazle, J., Whitney, J., and Diller, K. R., 2011, "Heat Shock Protein Expression and Temperature Distribution in Prostate Tumours Treated With Laser Irradiation and Nanoshells," Int. J. Hyperthermia, **27**(8), pp. 791–801.
[7] Bhowmick, S., Swanlund, D. J., and Bischof, J. C., 2000, "Supraphysiological Thermal Injury in Dunning AT-1 Prostate Tumor Cells," ASME J. Biomech. Eng., **122**(1), pp. 51–59.
[8] Hou, C. H., Hou, S. M., Hsueh, Y. S., Lin, J., Wu, C. H., and Lin, F. H., 2009, "The In Vivo Performance of Biomagnetic Hydroxyapatite Nanoparticles in Cancer Hyperthermia Therapy," Biomaterials, **30**(23), pp. 3956–3960.
[9] Kumar, V., Abbas, A., Nelson, F., and Mitchell, R., 2007, *Robbins Basic Pathology*, 8th ed., Elsevier/Saunders, Philadelphia, PA.
[10] Skinnider, L. F., and Ghadially, F. N., 1976, "Chloramphenicol-Induced Mitochondrial and Ultrastructural Changes in Hemopoietic Cells," Arch. Pathol. Lab., **100**(11), pp. 601–605.
[11] Fischer, A. H., Jacobson, K. A., Rose, J., and Zeller, R., 2008, "*Hematoxylin and Eosin Staining of Tissue and Cell Sections*," Cold Spring Harbor Protocols, **3**(5).
[12] LeBrun, A., Ma, R., and Zhu, L., 2016, "MicroCT Image Based Simulation to Design Heating Protocols in Magnetic Nanoparticle Hyperthermia for Cancer Treatment," J. Therm. Biol., **62**(Part B), pp. 129–137.
[13] LeBrun, A., Joglekar, T., Bieberich, C., Ma, R., and Zhu, L., 2016, "Identification of Infusion Strategy for Achieving Repeatable Nanoparticle Distribution and Quantification of Thermal Dosage Using MicroCT Hounsfield Unit in Magnetic Nanoparticle Hyperthermia," Int. J. Hyperthermia, **32**(2), pp. 132–143.
[14] Osborne, C. K., Hobbs, K., and Clark, G. M., 1985, "Effect of Estrogens and Antiestrogens on Growth of Human Breast Cancer Cells in Athymic Nude Mice," Cancer Res., **45**(2), pp. 584–590.
[15] Euhus, D. M., Hudd, C., LaRegina, M. C., and Johnson, F. E., 1986, "Tumor Measurement in the Nude Mouse," J. Surg. Oncol., **31**(4), pp. 229–234.
[16] Tomayko, M. M., and Reynolds, C. P., 1989, "Determination of Subcutaneous Tumor Size in Athymic (Nude) Mice," Cancer Chemother. Pharmacol., **24**(3), pp. 148–154.
[17] Manuchehrabadi, N., Attaluri, A., Cai, H., Edziah, R., Lalanne, E., Bieberich, C., Ma, R., Johnson, A. M., and Zhu, L., 2013, "Tumor Shrinkage Studies and Histological Analyses After Laser Photothermal Therapy Using Gold Nanorods," J. Biomed. Eng. Technol., **12**(2), pp. 157–175.
[18] Jensen, M. M., Jorgensen, T., Binderup, T., and Kjaer, A., 2008, "Tumor Volume in Subcutaneous Mouse Xenografts Measured by MicroCT is More Accurate and Reproducible Than Determined by 18F-FDG-MicroPET or External Caliper," BMC Med. Imaging, **8**(1), epub.
[19] Johannsen, M., Gneveckow, U., Thiesen, B., Taymoorian, K., Cho, C. H., Waldöfner, N., Scholz, R., Jordan, A., Stefan, A., Loening, S. A., and Wust, P., 2007, "Thermotherapy of Prostate Cancer Using Magnetic Nanoparticles: Feasibility, Imaging, and Three-Dimensional Temperature Distribution," Eur. Urol., **52**(6), pp. 1653–1662.
[20] Maier-Hauff, K., Ulrich, F., Nestler, D., Niehoff, H., Wust, P., Thiesen, B., Orawa, H., Budach, V., and Jordan, A., 2011, "Efficacy and Safety of Intratumoral Thermotherapy Using Magnetic Iron-Oxide Nanoparticles Combined With External Beam Radiotherapy on Patients With Recurrent Glioblastoma Multiforme," J. Neuro-Oncol., **103**(2), pp. 317–324.
[21] Maeda, H., 2001, "The Enhanced Permeability and Retention (EPR) Effect in Tumor Vasculature: The Key Role of Tumor-Selective Macromolecular Drug Targeting," Adv. Enzyme Regul., **41**(1), pp. 189–207.
[22] Singha, N., Jenkins, G. J. S., Asadi, R., and Doak, S. H., 2010, "Potential Toxicity of Superparamagnetic Iron Oxide Nanoparticles (SPION)," Nano Rev., **1**, p. 5358.
[23] Markides, H., Rotherham, M., and El Haj, A. J., 2012, "Biocompatibility and Toxicity of Magnetic Nanoparticles in Regenerative Medicine," J. Nanomater., 2012, p. 452767.
[24] Reddy, L. H., Arias, J. L., Nicolas, J., and Couvreur, P., 2012, "Magnetic Nanoparticles: Design and Characterization, Toxicity and Biocompatibility, Pharmaceutical and Biomedical Applications," Chem. Rev., **112**(11), pp. 5818–5878.
[25] Wust, P., Gneveckow, U., Johannsen, M., Bohmer, D., Henkel, T., Kahmann, F., Sehouli, J., Felix, R., Ricke, J., and Jordan, A., 2006, "Magnetic Nanoparticles for Interstitial Thermotherapy Feasibility, Tolerance and Achieved Temperatures," Int. J. Hyperthermia, **22**(8), pp. 673–685.
[26] Sadauskas, E., Wallin, H., Stoltenberg, M., Vogel, U., Doering, P., Larsen, A., and Danscher, G., 2007, "Kupffer Cells are Central in the Removal of Nanoparticles From the Organism," Part. Fibre Toxicol., **4**, epub.
[27] Moros, E., 2012, *Physics of Thermal Therapy: Fundamentals and Clinical Applications*, CRC Press, Boca Raton, FL.
[28] Chu, K. F., and Dupuy, D., 2014, "Thermal Ablation of Tumours: Biological Mechanisms and Advances in Therapy," Nat. Rev., **14**(3), pp. 199–208.
[29] Song, A. S., Najjar, A. M., and Diller, K. R., 2014, "Thermally Induced Apoptosis, Necrosis, and Heat Shock Protein Expression in 3D Culture," ASME J. Biomech. Eng., **136**(7), p. 071006.